

ANALYTICAL METHOD, MODELING AND BOUNDARY CONDITION FOR THE RESPONSE ANALYSIS WITH NONLINEAR SOIL-STRUCTURE INTERACTION

Kunihiko UNO¹, Hiroo SHIOJIRI², Kazuhiro KAWAGUCHI³ and Masataka NAKAMURA⁴

¹ Structural and Seismic Eng., Civil Eng. Design Div., Penta-Ocean Construction Co., Ltd., Tokyo, Japan
Email: Kunihiko.Uno@mail.penta-ocean.co.jp

² Professor, Dept. of Civil Eng., College of Science and Technology, Nihon University, Tokyo, Japan
Email: shiojiri@civil.cst.nihon-u.ac.jp

³ Deputy Division Manager, Structural Eng. Div., JIP Techno Science Corporation, Tokyo, Japan
Email: kawaguti@tokyo.jip-ts.co.jp

⁴ Assistant Assoc., Dept. of Civil Eng., College of Science and Technology, Nihon University, Tokyo, Japan
Email: masa@civil.cst.nihon-u.ac.jp

ABSTRACT :

Recently, as the structural design has shifted to the performance design, seismic design considering soil-structure interaction becomes more important. In this study, it is examined at first the difference between the frequency domain analysis and the time domain analysis. As a result, it was confirmed that frequency domain equivalent linear method is able to be applied to dynamic response analysis of steel structure, when the input earthquake motion is small. On the contrary, RC structure, with larger mass and higher stiffness, is subject to the larger effects of soil-structure interaction, and the results of the different modeling don't coincide well with each other. It needs more extensive meshes or sophisticated boundary conditions for such structure. Moreover, when extensive foundation soils become nonlinear due to strong earthquakes such that all nonlinear domains are not contained in FEM model, usual viscous boundary conditions cannot absorb outgoing wave well. The efficient PML boundary is proposed for linear and nonlinear FEM analysis. The analytical results are compared with those of extensive meshes and these results agree well. It shows good performances of these boundary conditions.

KEYWORDS: Soil-structure interaction, Analytical method, Boundary condition, FEM model, PML boundary

1. INTRODUCTION

The South Hyogo prefecture Earthquake in 1995 caused extensive damage to structures such as bridges, underground structures, harbor equipments and lifeline facilities, etc., and exerted large influences on the seismic design methods that had been enacted afterwards. Recently, as the structural design has shifted to the performance design¹⁾, seismic design considering soil-structure interaction is requested more through development of the computer technology and higher-need of realistic strain analysis.

There are two methods of seismic response analysis, frequency domain analysis and time domain analysis. Engineers should properly select analytical method to be used. In the FEM analysis, it is necessary to set the boundary condition to be able to model the ground that extends infinitely. However, the choices are limited when we use existing analysis tools, so we have to model large ground area, resulting in high computational cost²⁾.

In this study, the effects of the boundary condition and the range of modeling in the ground area on the response were examined firstly. Then, it is shown to be able to reduce the range of modeling in the ground area by proposed PML boundary.

2. ANALYTICAL METHOD AND BOUNDARY CONDITION

By discretizing space, simultaneous partial differential equations concerning coordinates and time are replaced by simultaneous ordinary differential equations with respect to time, and we obtain following simultaneous equations of multiple degree of freedom system in matrix form.

$$[M]\{\ddot{u}(t)\} + [C]\{\dot{u}(t)\} + [K]\{u(t)\} = \{f(t)\} \quad (2.1)$$

Usually we cannot solve them rigorously because they are simultaneous ordinary differential equations though they are similar in form to the motion equation of single degree of freedom system. In numerical time integration using Newmark's β method etc., they are replaced by simultaneous algebraic equations to solve it. On the other hand, by Fourier transforms of Eq.2.1, it is obtained the following Eq.2.2 that are complex simultaneous algebraic equations.

$$(-\omega^2[M] + i\omega[C] + [K])\{U(\omega)\} = \{F(\omega)\} \quad (2.2)$$

It is assumed to apply unit harmonic external force on each degree of freedom at a time, then, external forces of right side can be expressed as unit matrix [I], and the obtained solution becomes transfer function matrix [H(ω)]

$$(-\omega^2[M] + i\omega[C] + [K])\{H(\omega)\} = [I] \quad (2.3)$$

Then, time history response $\{u(t)\}$ is obtained as

$$\{u(t)\} = \frac{1}{2\pi} \int_{-\infty}^{\infty} [H(\omega)]\{F(\omega)\}e^{i\omega t} d\omega \quad (2.4)$$

Moreover, while damping is uniquely determined from $h \sim \gamma$ relationship in frequency domain analysis, the velocity proportional damping and the hysteresis damping usually exist in nonlinear behavior. It is difficult to express the frequency dependence of damping by velocity proportional damping, though the Rayleigh damping is widely used^(3),4),5),6).

As to the boundary condition, viscous boundary absorbs incidence energy of wave motion by a viscous stress in the boundary. However, the influence of the subgrade reaction that acts on the boundary is not clear because the viscous boundary absorbs the wave energy only by viscous stress. The frequency independent viscous boundary can be applied to the body wave (primary wave and secondary wave, etc.), but the viscous boundary that absorbs the surface wave, which exerts large influence by spreading of the wave energy in the ground level, must be functions of the frequency. Because the viscous boundary should be set at the distance in the same order as wavelength of Rayleigh wave from structure for base excitation, the computational data is huge to discretize using the FEM.

On the other hand, in frequency domain analysis, rigorous boundary conditions can be derived based on theoretical solution when foundation soil is discretized vertically. The boundary is called the energy transmission boundary.

As previously noted, it is thought to be necessary to examine the analytical methods and boundary conditions as above-mentioned, because the FEM analysis will become mainstream in seismic design.

3. ANALYTICAL MODEL

3.1. Object structure and modeling method

In this research, we examined the building shown in Photo 1. The structure is SRC building, 6 layer structure of rising 5 stories above the ground and 1 underground story.

The analytical model is shown in Figure 1. For the building, the element types are different for the above ground part, the underground part and the bottom slab. The above ground part is modeled by two dimensional beam element. All cross-sectional area and geometric moment of inertia of beams and columns in backward direction, are summed, and equivalent values for unit length in backward direction are assigned. Linear plane elements are used for the underground part and the bottom part. In addition, the pile foundations are modeled by two dimension beam element. Masses and stiffnesses of the pile are summed in the backward direction, and dividing them by the backward distance to get two dimensional material properties.

The properties of foundation are obtained by PS logging as shown in Figure 2 and by triaxial compression test as shown in Figure 3. The foundation soil is modeled by plane strain element.



Photo 1 Object building

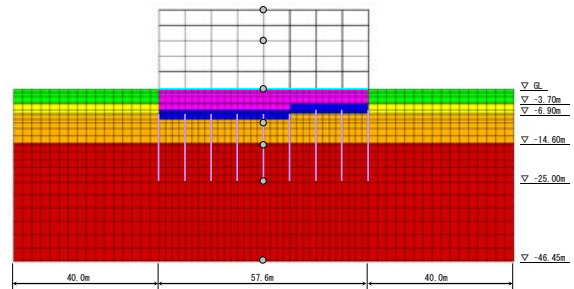


Figure 1 Analytical model

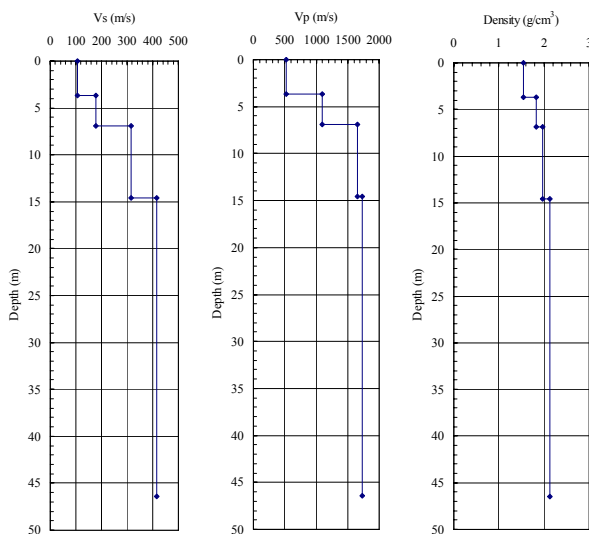


Figure 2 PS logging data

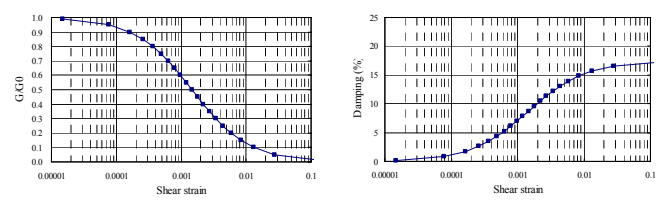


Figure 3 Triaxial compression test

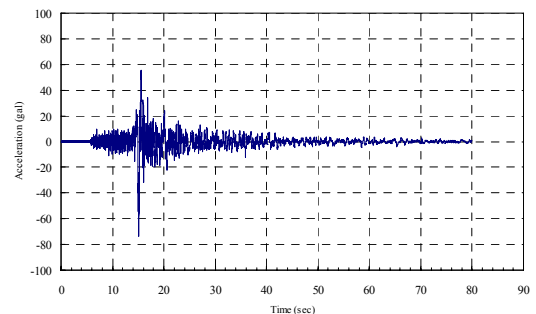


Figure 4 Input earthquake motion

3.2. Earthquake observed in object region

The seismograph is set up in the object structure and the ground right under, and the seismic observation has been conducted⁷⁾. The validity of the analytical model was first examined through comparison with the earthquake observation record.

The input earthquake motion is shown in Figure 4. This earthquake wave was observed with the seismograph in this building right under on July 23, 2005.

4. EFFECTS OF ANALYTICAL METHOD AND MODELING OF GROUND AREA ON THE OBSERVED EARTHQUAKE RESPONSES

The validity of an analytical model is verified by using the observed earthquake responses. The response values calculated by the analysis are compared with those observed with the seismograph set up in the building. Two kinds of the analytical methods, the frequency domain analysis and time domain analysis were executed, and the validity of the boundary condition etc. was verified.

The boundary condition on the side is the viscous boundary or the energy transmission boundary and the stress-strain relationship of the ground as shown in Figure 3 is used in the frequency domain analysis. In time domain analysis, the viscous boundary was similarly assumed, and τ - γ curve model of Hardin-Drnevich was used as the nonlinear model of the ground. Numerical integration was conducted using the integration method of Newmark's β method ($\beta=0.25$). The time increment was set to be 0.005 seconds and 2% damping was assumed

for the building and the pile (two dimension beam element) in the both methods. Rayleigh damping parameters are set using the main modes obtained by the eigenvalue analysis in time domain analysis. As for the analytical code, SuperFLUSH is used for the frequency domain analysis and DIANA is used for the time domain analysis.

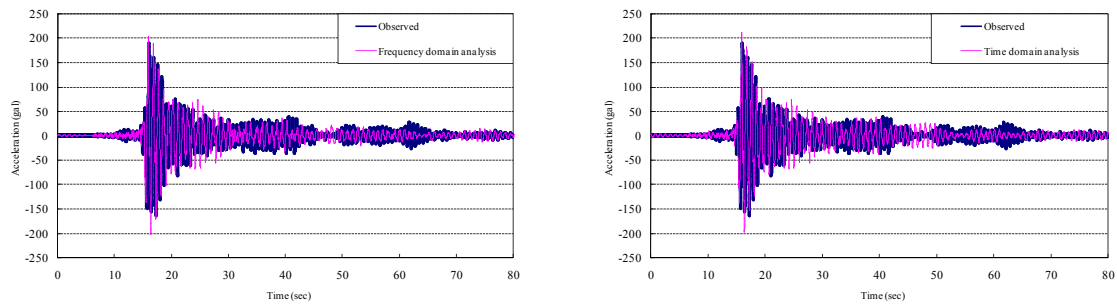


Figure 5 Comparison between observation value and analysis value

The analytical results are shown in Figure 5. The validity of the analytical model was examined by comparing the results of the response analyses of the frequency domain analysis and time domain analysis with observed ones. Agreements of computed results with observed ones are fairly good, though some differences are seen in the peak value of acceleration, which are considered to result from some damping discrepancy. Both analytical results in the frequency domain analyses and in time domain analysis are in good agreement. The generated strain in the ground is small because the energy of the input seismic motion is small, and it shows the frequency domain analysis (equivalent linear analysis) is good enough because the structure responses are within the range of elasticity.

The results of two kinds of boundary condition on the side, the energy transmission boundary and the viscous boundary, were almost the same in the frequency domain analysis. The results were also the same for the roller boundary and the periodical boundary in the time domain analysis when the building is SRC.

In addition, the influence of the range of modeling in the ground area was examined. The range of 40m was shown in Figure 1. The range of 10m, 20m and 40m from both ends of the building was modeled as the ground area. The effect of range on the response was small. The details of the result for comparative study are described in the next chapter.

5. EFFECT OF MODELING GROUND AREA WITH DIFFERENT SOIL-STRUCTURE INTERACTION

5.1. Modeling method of RC building

The influence of the modeled ground area on the analytical result is examined for the case, where the structure is changed from the current SRC building to the RC building, which has higher stiffness and larger mass. The stiffness and the mass of the RC building were calculated based on Building Code. The viscous boundary is set as a boundary condition. Analytical methods and other conditions are same as preceding chapter.

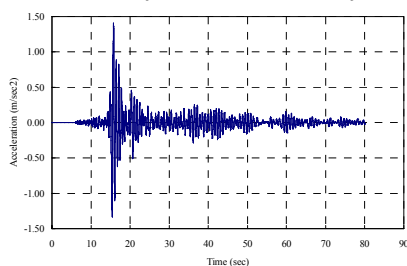


Figure 6 Time history of top of RC building (ground: 40m)

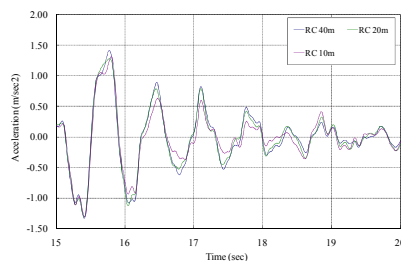


Figure 7 Comparison of the time histories of top of the RC building

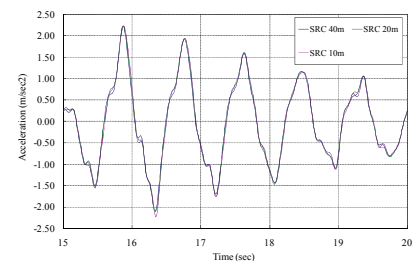


Figure 8 Comparison of the time histories of top of the SRC building

5.2. Analytical result

The analytical results are shown in Figure 6. The responses decrease more rapidly than those of SRC building. It is considered that the dynamic interaction is larger than that of SRC building due to larger mass and stiffness of

RC building. The responses between 15 sec and 20 sec of ground ranges 40m, 20m, and 10m were shown in detail in Figure 7. The results for the SRC building were similarly shown in Figure 8. It is clear that the influence of the ground area are larger for RC building compared to the SRC building. It is supposed that the influence of the boundary conditions on the behavior of the structure is larger for RC building than for SRC building.

6. EFFECT OF MODELING GROUND AREA FOR NONLINEAR RESPONSE

The influence of the ground area on the response is examined for the cases where the ground showed strong nonlinearity. The input seismic ground motion used is the record of the Kobe Port Island strong-motion seismograph (NS direction) in the South Hyogo prefecture Earthquake. The object structure is the RC building, and the Takeda-model is adopted for the nonlinear model of the material. The boundary condition used is the viscous boundary.

The acceleration time history of the top of the building, and 1F floor (A, B in Figure 9), as well as, the strain time history of the soil element (element C) which is right under the building are examined.

The response acceleration time histories between 15 sec to 20 sec of the building are shown in Figure 10 and Figure 11. The difference of the responses with the different the ground area is larger, because the ground shows strong nonlinearity due to the strong seismic motion and causes stronger interaction, and the building becomes also nonlinear.

The strain history curves of the ground are shown in Figure 12 ~ Figure 14. They also show the effect of range of the ground. It is considered that the effect of the range of the ground become larger as soil-structure interaction and nonlinearity of the ground or the structure get enhanced. It means that more sophisticated boundary such as PML is required if smaller range of the ground is used. The detail of PML is explained in the next chapter.

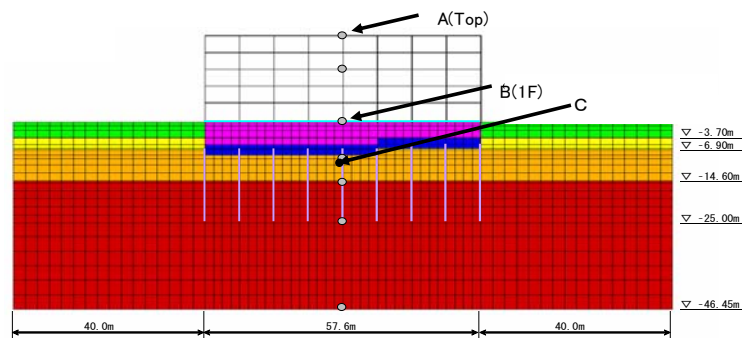


Figure 9 Analytical model and focus points (the case of ground area: 40m)

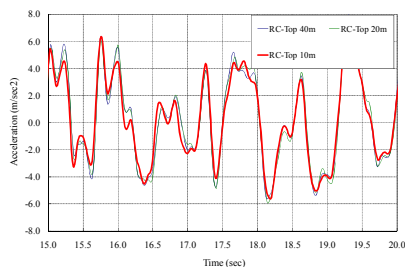


Figure 10 Comparison of time histories at top

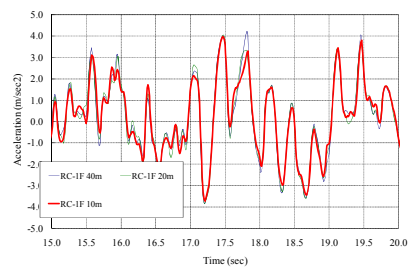


Figure 11 Comparison of time histories at 1F

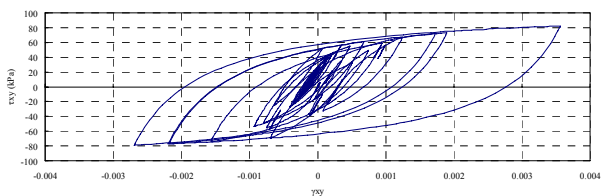


Figure 12 τ - γ history curve (C, ground: 40m)

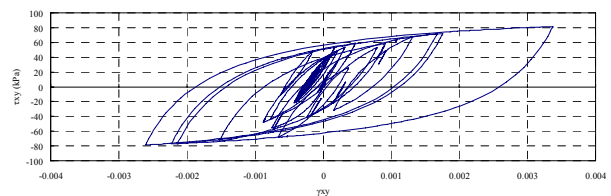


Figure 13 τ - γ history curve (C, ground: 20m)

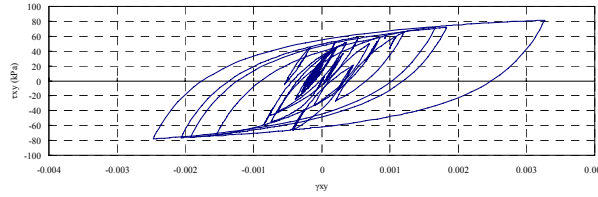


Figure 14 τ - γ history curve (C, ground: 10m)

7. PML BOUNDARY

7.1. PML implementation

PML is an artificial layer that is placed around the domain of interest, such that outgoing waves from the domain don't reflect at the interface due to the matching of impedances and that the amplitude of waves are reduced rapidly within the layer^{(8),(9),(10)}. Although PML was initially developed for the analysis of electromagnetic waves⁽⁸⁾, or ultrasonic waves⁽⁹⁾, where the ratio of traveling distances to wave length is extremely large, applications to elastic waves also have been conducted^{(10),(11),(12)}. Basu⁽¹¹⁾ formulated PML without field-splitting in frequency domain⁽¹¹⁾, which is consistent with FEM, and then developed PML implementation for transient analyses, in which unsymmetric tangent stiffness matrix was derived⁽¹²⁾.

Here, a formulation of PML for transient analysis of elastic waves is developed, in which tangent stiffness matrix is symmetric. Also developed is an implementation for vertically incident waves in FEM and PML. As Basu⁽¹¹⁾, we introduce complex coordinate stretching function in frequency domain analysis as:

$$\tilde{x}_i = \int_0^{x_i} \lambda_i(s) ds \quad (7.1)$$

, where x_i denotes i th coordinate, and \tilde{x}_i the corresponding transformed coordinate, and λ_i is given as:

$$\lambda_i(s) = 1 + f_i^e(s) + \frac{c_s}{i\omega b} f_i^p(s) \quad (7.2)$$

, where i is pure imaginary number, c_s shear wave velocity, b representative length, ω circular frequency, and f_i^e , f_i^p are non-dimensional non-negative continuous functions which are equal to 0 at FEM-PML interface.

At first, equations for elastic wave are formulated in \tilde{x}_i coordinate, and then transformed to x_i coordinate.

In two-dimensional case, it is written as⁽¹¹⁾ :

$$\frac{\partial \bar{\sigma}_{ij}}{\partial x_j} \left\{ 1 + f_i^e(x_i) + \frac{c_s}{i\omega b} f_i^p(x_i) \right\} = \quad (7.3.1)$$

$$-\omega^2 \rho \left\{ 1 + f_1^e(x_1) \right\} \left\{ 1 + f_2^e(x_2) \right\} \bar{u}_i + i\omega \rho \frac{c_s}{b} \left[\left\{ 1 + f_1^e(x_1) \right\} f_2^p(x_2) + \left\{ 1 + f_2^e(x_2) \right\} f_1^p(x_1) \right] \bar{u}_i + \rho \left(\frac{c_s}{b} \right)^2 f_1^p(x_1) f_2^p(x_2) \bar{u}_i$$

$$\bar{\sigma}_{ij} = C_{ijkl} \left(\bar{\varepsilon}_{kl} + i\omega \frac{2\zeta b}{c_s} \bar{\varepsilon}_{kl} \right) \quad (7.3.2)$$

$$\left\{ 1 + f_i^e(x_i) \right\} \left\{ 1 + f_j^e(x_j) \right\} \bar{\varepsilon}_{ij} + \frac{c_s}{i\omega b} \left[\left\{ 1 + f_i^e(x_i) \right\} f_j^p(x_j) + \left\{ 1 + f_j^e(x_j) \right\} f_i^p(x_i) \right] \bar{\varepsilon}_{ij} - \frac{1}{\omega^2} \left(\frac{c_s}{b} \right)^2 f_i^p(x_i) f_j^p(x_j) \bar{\varepsilon}_{ij}$$

$$= \frac{1}{2} \left[\left\{ 1 + f_i^e(x_i) \right\} \frac{\partial \bar{u}_i}{\partial x_j} + \left\{ 1 + f_j^e(x_j) \right\} \frac{\partial \bar{u}_j}{\partial x_i} \right] + \frac{c_s}{2i\omega b} \left\{ f_i^p(x_i) \frac{\partial \bar{u}_i}{\partial x_j} + f_j^p(x_j) \frac{\partial \bar{u}_j}{\partial x_i} \right\} \quad (7.3.3)$$

, where $\bar{\sigma}_{ij}$, \bar{u}_j , $\bar{\varepsilon}_{ij}$ are Fourier transforms of σ_{ij} , u_j , ε_{ij} , components of stresses, displacements and strains, respectively, and C_{ijkl} components of elastic tensor, ζ damping constant. Inverse Fourier transform of these equations gives equations in time domain⁽¹²⁾.

We develop weak form formulation in time domain, in which symmetric tangent stiffness matrix is derived.

Let Δt be time increment, $t_{n+1} = t_n + \Delta t$, $f(t)$ be an arbitral function, and γ, β be constants in Newmark

integration formulae. Then it can be assumed as:

$$\begin{aligned} \int_{t_n}^{t_{n+1}} f(t)dt &= (1-\gamma)\Delta t f(t_n) + \gamma\Delta t f(t_{n+1}) \\ \int_{t_n}^{t_{n+1}} \int_{t_n}^t f(t')dt'dt &= \beta\Delta t^2 f(t_{n+1}) + (1/2-\beta)\Delta t^2 f(t_n) + \Delta t \int_{t_n}^{t_n} f(t')dt' \end{aligned} \quad (7.3.4)$$

If we assume $\beta = \gamma^2$, and define g_j as: $g_j = \left\{1 + f_j^e(x_j) + \frac{c_s}{b}\gamma\Delta t f_j^p(x_j)\right\}$,

we obtain:

$$\frac{\partial \sigma_{ij}^{n+1}}{\partial x_j} g_{\check{x}} + \frac{c_s}{b} f_{\check{x}}^p(x_{\check{x}}) \left\{ (1-\gamma)\Delta t \frac{\partial \sigma_{ij}^n}{\partial x_j} + \frac{\partial \Sigma_{ij}^n}{\partial x_j} \right\} \quad (7.4.1)$$

$$\begin{aligned} &= \rho \left\{1 + f_1^e(x_1)\right\} \left\{1 + f_2^e(x_2)\right\} \ddot{u}_i + \rho \frac{c_s}{b} \left[\left\{1 + f_1^e(x_1)\right\} f_2^p(x_2) + \left\{1 + f_2^e(x_2)\right\} f_1^p(x_1) \right] \dot{u}_i + \rho \left(\frac{c_s}{b}\right)^2 f_1^p(x_1) f_2^p(x_2) u_i \\ &\quad \sigma_{ij} = C_{ijkl} \left(\varepsilon_{kl} + \frac{2\zeta b}{c_s} \dot{\varepsilon}_{kl} \right) \end{aligned} \quad (7.4.2)$$

$$\begin{aligned} &g_i g_j \hat{\varepsilon}_{ij}^{n+1} + \frac{c_s}{b} \left[\left\{1 + f_i^e(x_i)\right\} f_j^p(x_j) + \left\{1 + f_j^e(x_j)\right\} f_i^p(x_i) \right] \hat{\varepsilon}_{ij}^{n+1} + \left(\frac{c_s}{b}\right)^2 f_i^p(x_i) f_j^p(x_j) \hat{E}_{ij}^{n+1} \\ &= \frac{1}{2} \left[g_i \frac{\partial \hat{u}_i^{n+1}}{\partial x_j} + g_j \frac{\partial \hat{u}_j^{n+1}}{\partial x_i} \right] + \frac{c_s}{2b} \left[f_i^p(x_i) \frac{\partial \hat{u}_i^{n+1}}{\partial x_j} + f_j^p(x_j) \frac{\partial \hat{u}_j^{n+1}}{\partial x_i} \right] \end{aligned} \quad (7.4.3)$$

, and

$$\left. \begin{aligned} \hat{u}_k^{n+1} &= (1-\gamma)\Delta t \dot{u}_k^n + \frac{\partial u_k^n}{\partial x_l} \\ \hat{\varepsilon}_{ij}^{n+1} &= (1-\gamma)\Delta t \dot{\varepsilon}_{ij}^n + \varepsilon_{ij}^n \\ \hat{E}_{ij}^{n+1} &= (1-\gamma)\Delta t \dot{E}_{ij}^n + E_{ij}^n \end{aligned} \right\} \quad (7.4.4)$$

, where superscript n indicates value at time $n\Delta t$, Σ , E , U denote integral of stress, strain, and displacement, respectively, and \check{x} denotes other value than j. Let w_i be i component of weighing function, and we get weak form equations as:

$$\begin{aligned} &\int_S w_i n_j \left[\sigma_{ij}^{n+1} g_{\check{x}} + \frac{c_s}{b} f_{\check{x}}^p(x_{\check{x}}) \left\{ (1-\gamma)\Delta t \sigma_{ij}^n + \Sigma_{ij}^n \right\} \right] ds - \int_V \frac{\partial w_i}{\partial x_j} \left[g_{\check{x}} \sigma_{ij}^{n+1} + \frac{c_s}{b} f_{\check{x}}^p(x_{\check{x}}) \left\{ (1-\gamma)\Delta t \sigma_{ij}^n + \Sigma_{ij}^n \right\} \right] dv \\ &= \int_V w_i \rho \left\{1 + f_1^e(x_1)\right\} \left\{1 + f_2^e(x_2)\right\} \ddot{u}_i^{n+1} dv + \int_V w_i \rho \frac{c_s}{b} \left[\left\{1 + f_1^e(x_1)\right\} f_2^p(x_2) + \left\{1 + f_2^e(x_2)\right\} f_1^p(x_1) \right] \dot{u}_i^{n+1} dv \\ &\quad + \int_V \rho w_i \left(\frac{c_s}{b}\right)^2 f_1^p(x_1) f_2^p(x_2) u_i^{n+1} dv \end{aligned} \quad (7.5)$$

, where n_j is j component of unit outward normal vector of surface, and S and v are surface and volume of the domain, respectively. Inserting Eq.7.4.2, Eq.7.4.3 into Eq.7.5, we get equations for u_i^{n+1} as:

$$\begin{aligned} &\int_V \rho f_m w_i \ddot{u}_i dv + \int_V \rho f_e w_i \dot{u}_i dv + \left(\gamma\Delta t + \frac{2\zeta b}{c_s} \right) \int_V I g_j^{-1} g_l^{-1} C_{ijkl} \frac{\partial w_i}{\partial x_j} \frac{\partial \hat{u}_k^{n+1}}{\partial x_l} dv + \int_V w_i \rho f_k u_i dv \\ &= \int_S w_i n_j \left[I g_j^{-1} \sigma_{ij}^{n+1} + \frac{c_s}{b} f_{\check{x}}^p(x_{\check{x}}) \hat{\Sigma}_{ij}^n \right] ds - \int_V \frac{\partial w_i}{\partial x_j} \frac{c_s}{b} f_{\check{x}}^p(x_{\check{x}}) \hat{\Sigma}_{ij}^n dv \\ &\quad - \left(\gamma\Delta t + \frac{2\zeta b}{c_s} \right) \int_V I C_{ijkl} g_j^{-1} g_k^{-1} g_l^{-1} \frac{\partial w_i}{\partial x_j} \left[\frac{c_s}{b} f_k^p(x_k) \frac{\partial \hat{u}_k^{n+1}}{\partial x_l} \right. \\ &\quad \left. - \frac{2c_s}{b} \left\{1 + f_k^e(x_k)\right\} f_l^p(x_l) \hat{\varepsilon}_{kl}^{n+1} - \left(\frac{c_s}{b}\right)^2 f_k^p(x_k) f_l^p(x_l) \hat{E}_{kl}^{n+1} \right] dv - \int_V I C_{ijkl} g_j^{-1} \frac{\partial w_i}{\partial x_j} \hat{E}_{kl}^{n+1} dv \end{aligned} \quad (7.6)$$

, where

$$\left. \begin{aligned} I &= g_1 g_2 \\ f_m &= \{1 + f_1^e(x_1)\} \{1 + f_2^e(x_2)\} \\ f_c &= \frac{c_s}{b} \left[\{1 + f_1^e(x_1)\} f_2^p(x_2) \right. \\ &\quad \left. + \{1 + f_2^e(x_2)\} f_1^p(x_1) \right] \\ f_k &= \left(\frac{c_s}{b} \right)^2 f_1^p(x_1) f_2^p(x_2) \\ \hat{\Sigma}_{ij}^n &= (1 - \gamma) \Delta t \sigma_{ij}^n + \Sigma_{ij}^n \\ \frac{\partial \hat{u}_k^{n+1}}{\partial x_l} &= (1 - \gamma) \Delta t \frac{\partial \dot{u}_k^n}{\partial x_l} + \frac{\partial u_k^n}{\partial x_l} \\ \hat{\epsilon}_{ij}^{n+1} &= (1 - \gamma) \Delta t \dot{\epsilon}_{ij}^n + \epsilon_{ij}^n \end{aligned} \right\} \quad (7.7)$$

Introducing shape functions and discretizing the equations, and noting that weighing functions are arbitrary, we get equations for nodal displacements. Since the value of C_{ijkl} doesn't change if we change ij for kl mutually, tangential stiffness matrix is symmetric.

When both $f_i^e(x_i), f_i^p(x_i)$ equal to 0, resulting equations coincide with those for FEM.

7.2. Incident wave implementation

We assume incident wave is traveling in x_i direction. Within the domain where $\lambda_i = 1$, we set layer of 1 mesh width in x_i direction. Whole domain is divided by the layer into two part, i.e. object part and outer part. We assume in the layer, and in the outer part, superposition of stresses and displacements are possible. In object part, both incoming incident wave and scattering waves are considered, while only scattering waves are considered in outer part. In the layer, at nodal points on object part-layer boundary, both incident wave and scattering waves are considered, and only scattering waves are considered at nodal points on outer part-layer boundary. Incident wave is assumed to be known.

In calculating nodal forces of nodal points on object part-layer boundary, displacements corresponding to incident wave are added to those of nodal points on outer part-layer boundary. On the other hand, displacements etc. corresponding to incident wave are subtracted from those of nodal points on object part-layer boundary in calculating nodal forces of nodal points on outer part-layer boundary.

We denote displacement due to incident wave ${}^e u_i$, and the corresponding stresses and its integrated value ${}^e \sigma_{ij}^n, {}^e \Sigma_{ij}^n$. F_i^α , the nodal forces at nodal point α due to the incident wave displacement ${}^e u_i$, is given as:

$$\begin{aligned} F_i^\alpha &= - \int_v \frac{\partial N^\alpha}{\partial x_j} \left[g_{\chi\chi} {}^e \sigma_{ij}^{n+1} + \frac{c_s}{b} f_{\chi\chi}^p(x_{\chi\chi}) \{ (1 - \gamma) \Delta t {}^e \sigma_{ij}^n + {}^e \Sigma_{ij}^n \} \right] dv \\ &\quad - \int_v N^\alpha \rho f_m {}^e \ddot{u}_i^{n+1} dv - \int_v N^\alpha \rho f_c {}^e \dot{u}_i^{n+1} dv - \int_v N^\alpha \rho f_k u_i^{n+1} dv \end{aligned} \quad (7.8)$$

, where N^α is shape function for nodal point α . This force is added for nodal points on object part-layer boundary, where ${}^e u_i, {}^e \sigma_{ij}^n, {}^e \Sigma_{ij}^n$ correspond to nodal displacements on outer part-layer boundary due to incident wave, while it is subtracted for nodal points on outer part-layer boundary, where ${}^e u_i, {}^e \sigma_{ij}^n, {}^e \Sigma_{ij}^n$ correspond to nodal displacements due to incident wave on object part-layer boundary.

7.3. Numerical example

Responses of layered soil to vertical surface loading are calculated using small mesh with PML model, small mesh with viscous dampers, and extensive mesh. In Figure 15, small mesh model is illustrated.

Only right half is modeled, taking advantage of symmetry of the problem. In the model, all values are non-dimensional. Material properties are given in Table 1. Four noded quadrilateral elements with linear interpolation functions are used. Size of each element is 1x1. Ricker wavelet, $f(t)=\sqrt{\pi}\{1-2\pi(t/T)^2\}e^{-(t/T)^2}/T$ with $T=0.5$ is applied on the surface. Implicit integration of Newmark family with $\gamma=0.5, \beta=0.25$ is used for response computation. Time increment is 0.01. The responses of layerd soil at A to D are shown in Figure 16 ~ Figure 19. In those figures, 'reference' denotes responses of extensive mesh in which reflected waves do not come back during computed time, 'viscous' denotes viscous dampers. The performances of PML are shown to be better than those of viscous dampers.

Table 1 Material property

	layered soil	
	material 1	material 2
ρ	10	1
G	10000	1000

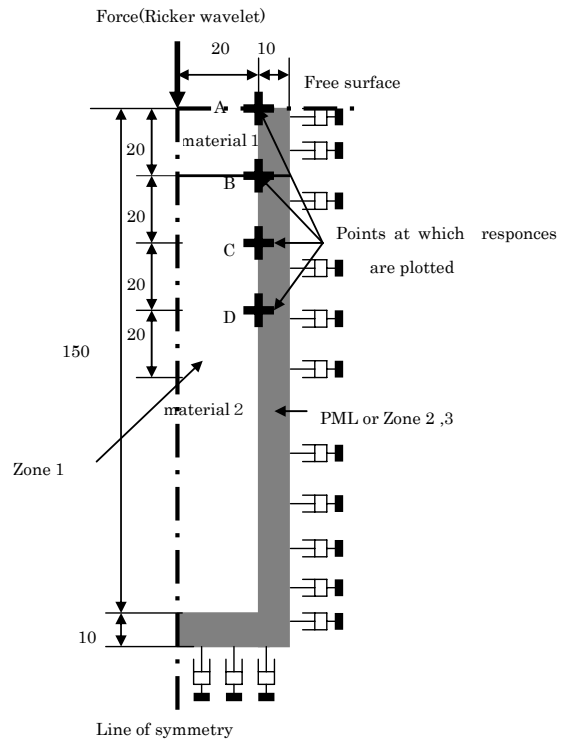


Figure 15 Soil model

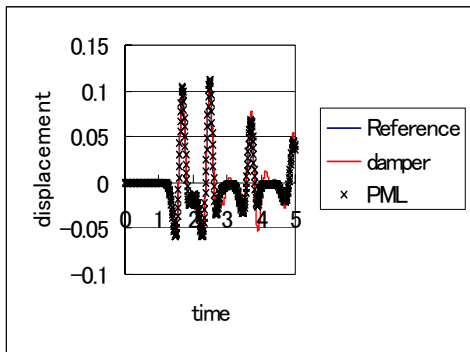


Figure 16 Response at A (layered soil)

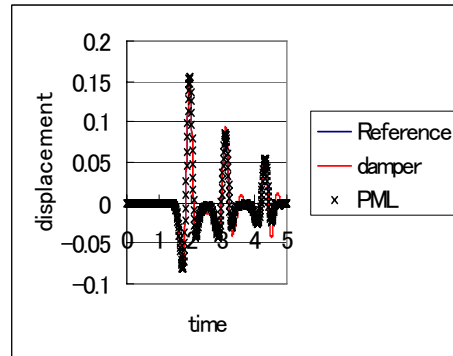


Figure 17 Response at B (layered soil)

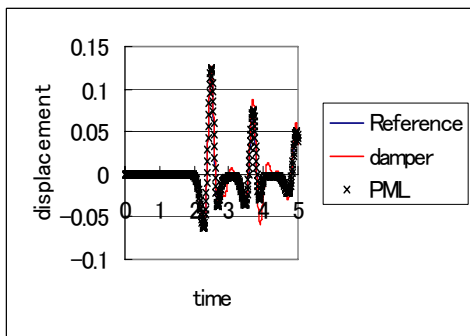


Figure 18 Response at C (layered soil)

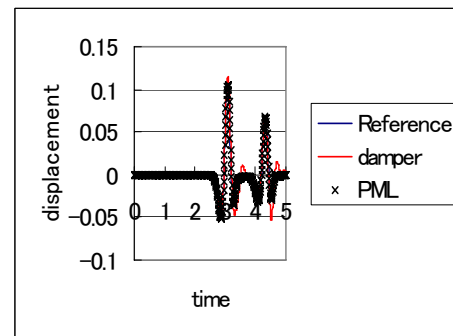


Figure 19 Response at D (layered soil)

7.4. Improvement of PML

The PML with complex coordinate stretching function given in Eq.7.2 may produce some error, when ω is small. We consider the following coordinate transfer function which has no singularity along real ω axis.

$$\lambda_i = k_i + \frac{\sigma_i}{\alpha_i + i\omega} \quad (7.9)$$

, where k_i, σ_i, α_i are functions of x_i only. Then equations of motion in PML are given as:

$$-\omega^2 \rho \bar{u}_i = \frac{1}{\lambda_j} \frac{\partial \bar{\sigma}_{ij}}{\partial x_j} \quad (7.10)$$

And strains are given as:

$$\bar{f}_{ij} = \frac{1}{\lambda_j} \frac{\partial \bar{u}_i}{\partial x_j}, \quad \bar{\varepsilon}_{ij} = \frac{1}{2} (\bar{f}_{ij} + \bar{f}_{ji}) \quad (7.11)$$

Stress-strain relationship is assumed as:

$$\bar{\sigma}_{ij} = C_{ijkl} \bar{f}_{kl} + D_{ijpqrsmn} \bar{f}_{pq} \bar{f}_{rs} \bar{f}_{mn} \quad (7.12)$$

In two-dimensional problem, multiplying Eq.7.10 with $\lambda_1 \lambda_2$, we obtain the following equations.

$$-\rho \omega^2 (k_1 + \frac{\sigma_1}{\alpha_1 + i\omega})(k_2 + \frac{\sigma_2}{\alpha_2 + i\omega}) \bar{u}_i = (k_j + \frac{\sigma_j}{\alpha_j + i\omega}) \frac{\partial \bar{\sigma}_{ij}}{\partial x_j} \quad (7.13)$$

Expanding, rearranging, and multiplying with weighing function w_i , we get weak form Equations as:

$$\begin{aligned} & \int_v -\rho \omega^2 w_i \left\{ k_1 k_2 + \frac{k_2 \sigma_1 (\alpha_2 - \alpha_1) + \sigma_1 \sigma_2}{(\alpha_2 - \alpha_1)(\alpha_2 + i\omega)} + \frac{k_1 \sigma_2 (\alpha_2 - \alpha_1) - \sigma_1 \sigma_2}{(\alpha_2 - \alpha_1)(\alpha_2 + i\omega)} \right\} \bar{u}_i dv \\ & = \int w_i (k_j + \frac{\sigma_j}{\alpha_j + i\omega}) \bar{\sigma}_{ij} n_j ds - \int \frac{\partial w_i}{\partial x_j} (k_j + \frac{\sigma_j}{\alpha_j + i\omega}) \bar{\sigma}_{ij}^i dv \end{aligned} \quad (7.14)$$

Using inverse Fourier transform, we obtain:

$$\begin{aligned} & \int_v \rho w_i \left\{ k_1 k_2 \ddot{u}_i + \frac{k_2 \sigma_1 (\alpha_2 - \alpha_1) + \sigma_1 \sigma_2}{\alpha_2 - \alpha_1} e^{-\alpha_1 t} * \ddot{u}_i + \frac{k_1 \sigma_2 (\alpha_2 - \alpha_1) - \sigma_1 \sigma_2}{\alpha_2 - \alpha_1} e^{-\alpha_2 t} * \ddot{u}_i \right\} dv \\ & = \int w_i (k_j \sigma_{ij} + \sigma_j e^{-\alpha_j t} * \sigma_{ij} n_j) ds - \int \frac{\partial w_i}{\partial x_j} (k_j \sigma_{ij} + \sigma_j e^{-\alpha_j t} * \sigma_{ij}) dv \end{aligned} \quad (7.15)$$

, where $*$ denotes convolution integral. Similarly, from Eq.7.11, we obtain:

$$k_j f_{ij} \sigma_j e^{-\alpha_j t} * f_{ij} = \frac{\partial u_i}{\partial x_j} \quad (7.16)$$

If we define function $F(t)$ as $F(t) = e^{-\alpha t} * f(t) = \int_0^t e^{-\alpha(t-t')} f(t') dt'$, then $F(t + \Delta t)$ can be approximated as:

$$\begin{aligned} F(t + \Delta t) &= \int_0^{t+\Delta t} e^{-\alpha(t+\Delta t-t')} f(t') dt' + e^{-\alpha \Delta t} \int_0^t e^{-\alpha(t-t')} f(t') dt' \\ &= \theta \Delta t f(t + \Delta t) + e^{-\alpha \Delta t} F^*(t) \end{aligned} \quad (7.17)$$

, where $0 \leq \theta \leq 1$, $F_{(t)}^* = F(t) + (1 - \theta) \Delta t f(t)$.

From Eq.7.15 and Eq.7.17, we obtain:

$$\begin{aligned} & \int_v \rho w_i \{ k_1 k_2 + \theta \Delta t (k_2 \sigma_1 + k_1 \sigma_2) \} \ddot{u}_i(t + \Delta t) dv \\ & - \int_v \rho w_i \left\{ (k_2 \sigma_1 + \frac{\sigma_1 \sigma_2}{\alpha_2 - \alpha_1}) e^{-\alpha_1 \Delta t} U_{i1}^*(t) + (k_1 \sigma_2 - \frac{\sigma_1 \sigma_2}{\alpha_1 - \alpha_2}) e^{-\alpha_2 \Delta t} U_{i2}^*(t) \right\} dv \\ & = \int w_i (k_j \sigma_{ij} + \sigma_j e^{-\alpha_j t} * \sigma_{ij} n_j) ds \\ & - \int \frac{\partial w_i}{\partial x_j} \left\{ (k_j + \theta \Delta t \sigma_j) \sigma_{ij}(t + \Delta t) + \sigma_j e^{-\alpha_j \Delta t} \sum_{ij}^*(t) \right\} dv \end{aligned} \quad (7.18)$$

, where $u_{i1}^*(t) = \int_0^t e^{-\alpha_1(t-t')} \ddot{u}_i(t') dt' + \Delta t (1 - \theta) \ddot{u}_i(t)$, $u_{i2}^* = \int_0^t e^{-\alpha_2(t-t')} \ddot{u}_i(t') dt' + \Delta t (1 - \theta) \ddot{u}_i(t)$, and

$$\sum_{ij}^* = \int_0^t e^{-\alpha_j(t-t')} \sigma_{ij}(t') dt' + \Delta t (1 - \theta) \sigma_{ij}(t)$$

For linear problem, above equations can be expressed as:

$$\begin{aligned}
 & \int_{\bar{v}} p w_i \{k_1 k_2 + \theta \Delta t (k_2 \sigma_1 + k_1 \sigma_2)\} \ddot{u}_i(t + \Delta t) dv + \int \frac{\partial w_i}{\partial x_j} \frac{DI}{g'_j g'_i} C_{ijkl} \frac{\partial u_k}{\partial x_l}(t + \Delta t) dv \\
 & = \int w_i (k_j \sigma_{ij} + \sigma_j e^{-\alpha_j t} * \sigma_{ij} n_j) ds \\
 & - \int_{\bar{v}} p w_i \left\{ \left(k_2 \sigma_1 + \frac{\sigma_1 \sigma_2}{\alpha_2 - \alpha_1} \right) e^{-\alpha_1 \Delta t} U_{i1}^*(t) + \left(k_1 \sigma_2 - \frac{\sigma_1 \sigma_2}{\alpha_2 - \alpha_1} \right) e^{-\alpha_2 \Delta t} U_{i2}^*(t) \right\} dv \\
 & - \int \frac{\partial w_i}{\partial x_j} \sigma_j e^{-\alpha_j \Delta t} \sum_{ij}^* (t) dv + \int \frac{\partial w_i}{\partial x_j} \frac{DI}{g'_j g'_i} C_{ijkl} e^{-\alpha_j \Delta t} \sigma_l F_{kl}^*
 \end{aligned} \tag{7.19}$$

, where $g'_j = k_j + \theta \Delta t \sigma_j$, $DI = g'_1 g'_2$. Again, we obtain symmetric tangent stiffness matrix.

7.5. Numerical example

We consider one dimensional rod shown in Figure 20. The stress-strain relationship is assumed as

$$\sigma_{11} = (\lambda + 2G)(f_{11} + b f_{11}^3).$$

Other parameters are assumed as:

$$\begin{aligned}
 \alpha_1 &= \frac{x}{L_p} \alpha_{MAX}, \quad \sigma_1 = \frac{x}{L_p} \sigma_{MAX}, \quad \kappa_1 = 1 + \frac{x}{L_p} \kappa_{MAX}, \\
 \alpha_{MAX} &= 1, \quad \sigma_{MAX} = 10, \quad \kappa_{MAX} = 10
 \end{aligned}$$

, where origin of x is set at PML-FEM interface. We impose displacement at the left end of the rod. The displacement is time-harmonic with amplitude $\sqrt{\pi}/10$, period 10, and duration 110. Mesh length is 1, $L=100$, $L_p=30$, $b=300$, or 0 (Linear), $\rho=1$, $\lambda=0$, $G=12.5$. Time histories at $x=0$ are shown in Figure 21 and Figure 22 along with those obtained with viscous dashpots set at right end. While performance of viscous dashpot is excellent in linear case ($b=0$), reflected wave is much smaller with PML than with viscous dashpots in nonlinear case ($b=300$).

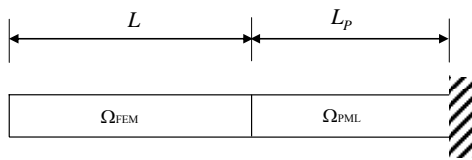


Figure 20 1-D model

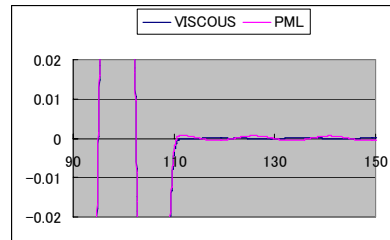


Figure 21 Comparison of displacement (linear) T=15

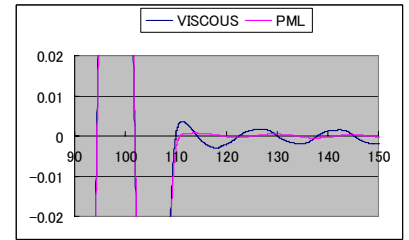


Figure 22 Comparison of displacement (nonlinear) T=15

8. CONCLUSIONS

Two kinds of the analytical methods, the frequency domain analysis and time domain analysis were used, and the validity of the boundary condition etc. was examined. Analytical results for SRC building both in the frequency domain analysis and in time domain analysis are in good agreement with observed ones. The generated strain in the ground is small because the energy of the input seismic motion is small, and the frequency domain analysis (equivalent linear analysis) is shown to be good enough because the structure responses are within the range of elasticity. The effect of range on the response was also small.

The effect of the modeled ground area on the analytical result of RC building, which has higher stiffness and larger mass, is larger than those for SRC building.

When larger seismic motion is applied, the difference of the responses with the different the ground area becomes larger, because the ground shows strong nonlinearity and the building becomes also nonlinear. It is considered that the effect of the range of the ground become larger as soil-structure interaction and nonlinearity of the ground or the structure get enhanced.

Simple and Efficient displacement based PML procedures have been developed for application to dynamic response analyses of semi-infinite soil-structure interaction problems in time domain. It is demonstrated by

numerical examples that the accuracies of the developed procedures are significantly better than that of viscous boundaries for both uniform and layered semi-infinite soil. Improved PML is applied to a non-linear problem and good performance is observed.

ACKNOWLEDGEMENTS

This research was conducted as a part of the Academically Promoted Frontier Research Program on “Sustainable City Based on Environmental Preservation and Disaster Prevention” at Nihon University, College of Science and Technology under a Grant from the Ministry of Education, Science and Sports, Japan.

REFERENCES

- 1) Japan Road Association: “Specifications for Highway Bridge Part V Seismic Design”, 1996
- 2) Kunihiko UNO, Hiroo SHIOJIRI, Kazuhiro KAWAGUCHI, Masataka NAKAMURA, Tomohiro NAKAHARA, Takamitsu OSHIMA: Influence of analytical method and boundary condition on dynamic behavior of soil-pile-structure systems, *JSCE Journal of Earthquake Engineering*, Vol.29, pp.1151-1158, 2007
- 3) Nozomu YOSHIDA, Sumio SAWADA, Susumu NAKAMURA: Effect of damping on earthquake response of ground and its accuracy, *Journal of JAEE*, Vol.6, No.4, pp.55-73, 2006
- 4) Taiji MAZDA, Hisanori OTSUKA, Kunihiko UNO: Speculation of evaluation of damping performance for PC rigid frame bridge, *Proceedings of the 7th symposium on ductility design method for bridges*, pp.143-148, 2004
- 5) Kunihiko UNO, Taiji MAZDA, Hisanori OTSUKA: Speculation of evaluation of damping performance for reaction force dispersed structure using rubber bearing, *Proceedings of the 8th symposium on ductility design method for bridges*, pp.61-68, 2005
- 6) Kunihiko UNO, Taiji MAZDA, Hisanori OTSUKA: Evaluation of influence of damping set during earthquake for reaction force dispersed structure using rubber bearing, *2005 Annual Meeting of Seibu Branch of JSCE, Part 1*, pp.137-138, 2005
- 7) Earthquake observation system in Funabashi area, the state and the data management: *Journal of the research institute of science and technology*, Nihon University, No.112, 2006
- 8) J.P.Berenger: A Perfectly Matched Layer for the Absorption of Electromagnetic Waves, *Journal of Computational Physics*, No.114, pp.185-200, 1994.
- 9) Daiji FUJII, Norihito UETSUKI, Katsuyuki SUZUKI, and Hideomi OHTSUBO: Wave propagation analysis of ultrasound using voxel finite element method and PML absorbing boundary, *Transactions of JSCEs*, No.20010015, p.8, 2001
- 10) F.Collino and C.Tsogka: Application of the perfectly matched absorbing layer to the linear elastodynamic problem in anisotropic heterogeneous media, *Geophysics* 66 (1), 294-307. 2001
- 11) U.Basu and A.K.Chopra: Perfectly matched layers for time-harmonic elastodynamics of unbounded domains: theory and finite-element implementation, *Comput. Methods Appl. Mech. Eng.*192, pp1337-1375, 2003,
- 12) U.Basu and A.K.Chopra: Perfectly matched layers transient elastodynamics of unbounded domains, *Int.J.Numerical Methods Eng.*59, pp1039-1074, 2004